Applied Catalysis A, General 608 (2020) 117838

Contents lists available at ScienceDirect

Applied Catalysis A, General

journal homepage: www.elsevier.com/locate/apcata

Co-Ru catalysts with different composite oxide supports for Fischer–Tropsch studies in 3D-printed stainless steel microreactors

S. Bepari[a], Xin Li[b], R. Abrokwah[a], N. Mohammad[b], M. Arslan[a], D. Kuila[a,b,*]

[a] Chemistry Department, Applied Sciences and Technology, Greensboro, NC, 27411, United States
[b] Joint School of Nanoscience and Nanoengineering, North Carolina A&T State University, Greensboro, NC, 27411, United States

ARTICLE INFO

Keywords:
FT synthesis
CoRu catalyst
Mesoporous composite oxide
SS microreactor
Silica-alumina
Alumina-titania

ABSTRACT

Bimetallic Co-Ru on different mesoporous composite oxides (m-SiO_2-Al_2O_3, m-SiO_2-TiO_2, m-TiO_2-Al_2O_3) and CoRu-m-SiO_2-TiO_2 were synthesized by incipient wet-impregnation (IWI) and one-pot (OP) hydrothermal methods, respectively. Bimetallic catalysts were coated in the microchannels of 3D-printed stainless steel (SS) microreactors for Fischer-Tropsch (FT) studies. The physiochemical properties of the catalysts were examined by BET, XRD, SEM, TEM, TPR, TGA-DSC and XPS techniques. The TPR results showed that the method and the composite support had a profound effect on the reducibility of the active sites. All the catalysts resisted deactivation for first 50 h and 10Co5Ru/m-SiO_2-TiO_2 (IWI) was most stable with ~80 % CO conversion at the end of 60 h. The stability and activity of the catalysts were observed in the order: 10Co5Ru/m-SiO_2-TiO_2 (IWI) > 10Co5Ru/m-SiO_2-Al_2O_3 (IWI) > 10Co5Ru/m-Al_2O_3-TiO_2 (IWI) > 10Co5Ru-m-SiO_2-TiO_2 (OP). The TPO and XRD analyses of the spent catalysts confirmed coking as a potential factor but not the only cause of catalyst deactivation over time.

1. Introduction

Depletion of petroleum resources, oil price fluctuation and global warming have triggered researchers to focus on new approaches to produce clean fuels [1]. Fischer–Tropsch synthesis (FTS) is the process to generate liquid fuels from syngas (mixture of CO and H_2) obtained from oil-alternative resources such as natural gas (Gas To Liquid, GTL), coal (Coal To Liquid, CTL) and biomass (Biomass To Liquid, BTL) [2]. The product selectivity of fuel and CO conversion depend on physiochemical features of the catalyst and reaction conditions [3]. In this regard, Co-based catalysts are most attractive to produce linear hydrocarbons with C_{5+} chain length due to their high activity, good stability and low water-gas shift activity [4,5]. The activity of the catalyst depends on several factors such as Co-particle size, the support, the presence of promoters, preparation method and pre-treatment conditions [6]. Porous inorganic oxide supports with high surface area such as SiO_2, Al_2O_3 and TiO_2 are generally used to prepare Co-based catalysts [7]. Some researchers have investigated SiO_2 as support for FTS due to its good stability and adequate porosity [8–10]. Other supports such as TiO_2 have been reported to promote the formation of C_2 oxygenates [11,12]. Alumina has also been utilized as supports for Co-based FT catalysts because of its high thermal stability and the strong resistance to attrition [13]. It also provides stable catalytic activity for a longer period due to the ability of Al_2O_3 support to stabilize small metal clusters which would suppress the aggregation of Co-metal particles during the reaction [13].

Mesoporous materials have been successfully used as support for Co-based catalyst due to their high surface areas and uniform pore size distribution. The mesoporous nature of the support would help to maximize the dispersion of active metal along with thermal, mechanical and chemical stability of the FT catalyst [14]. Another advantage of a mesoporous-structured catalyst is to provide maximum contact time between active metal and reaction gas molecules [14]. The composite metal oxide would facilitate CO conversion and product selectivity by tuning the structural stability of the catalyst. The small particle size of Co in the support is hampered by reducibility of the catalyst. In order to enhance the reducibility and dispersion of Co particles, some transition metals (e.g. Ni, Cu, Mo, V, Cr, Nb, Zr, Ti) including noble metals (e.g. Ru, Re, Ir, Pd, Rh, Os, Au, Ag and Pt), rare earth metals (e.g. Ce, La, Sc, Pr, Y), and alkali and alkaline earth metals (e.g. Li, Na, K, Rb, Cs, Ca and Mg) have been used as a promoter for the supported Co-based catalysts [15–25]. Some parameters which influence the promotional effect of the elements on Co-based catalyst are: (1) the nature of the support and its textural properties, (2) promoter and Co-loading, (3) synthesis method of the catalyst and (4) FTS reaction conditions [26]. These parameters affect the active site, catalyst stability and Co-support

* Corresponding author.
E-mail address: dkuila@ncat.edu (D. Kuila).

https://doi.org/10.1016/j.apcata.2020.117838
Received 2 March 2020; Received in revised form 13 September 2020; Accepted 17 September 2020
Available online 20 September 2020
0926-860X/

interaction. However, it may be difficult to judge the effect of the promoter on the activity of Co-based catalyst [17,18].

Apart from the catalyst, the type of reactor also plays an important role in FTS. The conventional reactor systems such as a tubular fixed-bed reactor (TFBR), micro-fixed bed reactor and continuous stirred-tank reactor (CSTR) have been widely used in FTS [26–29]. The Pearl and Qatar petroleum corporation is working on GTL technology to produce 140000 bpd (barrel per day), which is an example of the profitable economical scale of GTL processing [30]. There are some limitations of the scale-up considerations to commercialize small scale industry into a profitable process. This limitation has driven both industry and researchers to find alternative technologies. Microstructured technology is considered as an alternative for small and medium scale catalytic processes. Many researchers and industries such as Velocys and Micromeritics have been actively doing research in this area [31–33]. However, very limited use of a microchannel microreactor has been reported for FTS [34–38]. The use of microreactor is gaining attention for FTS due to its high heat dissipation for exothermic reactions, efficient mass transfer, high reaction throughput, precise control of hydrodynamics, portability and easy scale-up [39–43] of the reactions.

In this present work, three mesoporous oxide composites have been investigated as supports for Ru promoted Co-based catalyst in FTS. Mesoporous SiO_2-TiO_2 composite oxide is considered because SiO_2 tends to avail a large surface area and improves CO adsorption and TiO_2 enhances the formation of C_2 oxygenates [44]. Similarly, Al_2O_3 is another good support for FT reaction due to its favorable mechanical and tunable properties [45]. However, the strong interaction between the Co-ion and Al_2O_3 decreases reducibility of the metal. Incorporation of both SiO_2 and Al_2O_3 can therefore optimize support properties and can increase the reducibility of the Co catalyst [46]. Another important reason for selecting the mesoporous composite supports is to explore any synergistic effects of the supports on catalyst activity [47]. Usually a small amount of ruthenium is added to cobalt catalysts to increase reducibility and dispersion of Co active sites. The physiochemical properties of all catalysts were characterized by several characterization techniques such as N_2 adsorption-desorption isotherm, H_2-temperature programmed reduction (H_2-TPR), X-ray diffraction (XRD), Transmission electron microscopy (TEM), Scanning electron microscopy (SEM) with energy dispersive spectroscopy (EDS) and X-ray photoelectron spectroscopy (XPS). All Co-based catalysts were tested to measure their catalytic activities in terms of syngas or CO conversion and product selectivity for FTS in 3D printed stainless steel (SS) microchannel microreactors.

2. Experimental methods

2.1. Materials

For the mesoporous composite support synthesis, aluminum isopropoxide $C_9H_{21}O_3Al$, tetraethyl orthosilicate (TEOS) and titanium isopropoxide (TIPR) as a precursor of alumina, SiO_2 and TiO_2 were purchased from Sigma-Aldrich, USA. Pluronic P123 as a structure agent and Cetyl trimethyl ammonium bromide (CTAB) were also procured from Sigma-Aldrich, USA. Anhydrous ethanol and hydrochloric acid (HCl) were purchased from Fischer Scientific, USA. The active metals precursors, cobalt nitrate hexahydrate [$Co(NO_3)_2.6H_2O$] and Ruthenium Chloride [$RuCl_3$. xH_2O], were acquired from Alfa Aesar, USA. Deionized water (DI water) was used as a solvent.

2.2. Different support synthesis

2.2.1. Mesoporous SiO_2-TiO_2 (m-SiO_2-TiO_2) support

Mesoporous SiO_2-TiO_2 was prepared using a one-pot process with TEOS as the limiting reagent [48,49]. In an actual preparation, the molar composition of the reagents used was 1 TEOS: 0.752 TIPR 0.081 CTAB: 41 H_2O: 7.5 ethanol: 0.01679 Pl23: 5.981 HCl. For a typical synthesis (to obtain 10 g of the catalyst after calcination); first, P123 was dissolved in 2 M HCl at 35 °C to obtain a clear solution designated as solution “A”. A second solution designated as “B” was prepared by dissolving CTAB in DI water and stirring at 35 °C until a colorless solution was obtained. Solution B was then gently poured into solution A while stirring for 30 min. Ethanol was gently added to the resulting mixture. TEOS and TIPR were mixed and stirred in a separate beaker to obtain a yellow solution and then added dropwise to the mixture while stirring vigorously. This final mixture was covered with parafilm and stirred for 20 h at 35 °C for aging under the fume hood. The final aqueous mixture with pH = 1 was then aged at 80 °C in the oven for at least 48 h (to dry) followed by air-drying under a fume hood for 24 h. The sample (now a yellowish-white precipitate) was then oven-dried again for 24 h at 98 °C. Finally, the dried material was calcined in a furnace under air at 550 °C for 6 h.

2.2.2. Mesoporous Al_2O_3-TiO_2 (m-Al_2O_3-TiO_2) support

Mesoporous Al_2O_3-TiO_2 was prepared using a one-pot process with TIPR as the limiting reagent [47,49]. The molar composition of the reagents used was 1 TIPR: 0.783 $C_9H_{21}O_3Al$ 0.081 CTAB: 41 H_2O: 7.5 ethanol: 0.0167 Pl23: 5.981 HCl. For a typical synthesis (to obtain 10 g of the catalyst after calcination); first, P123 was dissolved in 2 M HCl at 35 °C to obtain a clear solution designated as solution “A”. A second solution designated as “B” was prepared by dissolving CTAB in DI water and stirring at 35 °C until a colorless solution was obtained. Solution B was then gently poured into solution A while stirring for 30 min to obtain mixture C. In a separate beaker $C_9H_{21}O_3Al$ was dissolved/stirred in ethanol and heated at 80 °C until complete dissolution. The dissolved $C_9H_{21}O_3Al$ was added to TIPR and stirred vigorously to prevent precipitation and was designated solution ‘D’. Solution D which was quite viscous was then added dropwise to the mixture ‘C’ and stirred vigorously. This final mixture was covered with parafilm and stirred for 20 h at 35 °C for aging under the fume hood. The final aqueous mixture with pH = 0.5 was then aged at 80 °C in the oven for at least 48 h (to dry) followed by air-drying under a fume hood for 24 h. The sample (now a greyish precipitate) was then oven-dried again for 24 h at 98 °C. Finally, the dried material was calcined in a furnace under air at 400 °C for 4 h.

2.2.3. Mesoporous SiO_2-Al_2O_3 (m- SiO_2-Al_2O_3) support

Mesoporous SiO_2-Al_2O_3 was prepared using a one-pot process with TEOS as the limiting reagent [47,48]. In an actual preparation, the molar composition of the reagents used was 1 TEOS: 0.589 $C_9H_{21}O_3Al$ 0.081 CTAB: 41 H_2O: 7.5 ethanol: 0.0167 Pl23: 5.981 HCl. For a typical synthesis (to obtain 10 g of the catalyst after calcination); the first P123 was dissolved in 2 M HCl at 35 °C to obtain a clear solution designated as solution “A”. A second solution designated as “B” was prepared by dissolving CTAB in DI water and stirring at 35 °C until a colorless solution was obtained. Solution B was then gently poured into solution A while stirring for 30 min to obtain mixture C. In a separate beaker $C_9H_{21}O_3Al$ was dissolved/stirred in ethanol and heated at 80 °C until complete dissolution. The dissolved $C_9H_{21}O_3Al$ was added to TEOS and stirred vigorously to prevent precipitation and was designated solution ‘D’. Solution D which was quite viscous was then added dropwise to the mixture ‘C’ and stirred vigorously. This final mixture was covered with parafilm and stirred for 20 h at 35 °C for aging under the fume hood. The final aqueous mixture with pH = 1.5 was then aged at 80 °C in the oven for at least 48 h (to dry) followed by air-drying under a fume hood for 24 h. The sample (now a greyish precipitate) was then oven-dried again for 24 h at 98 °C. Finally, the dried material was calcined in a furnace under air at 550 °C for 6 h.

2.2.4. One-pot synthesis of mesoporous Co-Ru-m-SiO_2-TiO_2

Cobalt-ruthenium based bi-metallic nanocatalysts supported by composite oxides of SiO_2 and TiO_2 were synthesized using a one-pot hydrothermal procedure. TEOS, TIPR, P123, HCl were used in a molar ratio of 1: 0.752: 0.081: 41: 7.5: 0.01679: 5.981, respectively. The

quantity of metal precursor was calculated based on the weight percentage of metal to be incorporated into the catalysts. In a typical synthesis process, the weighed surfactant (CTAB) was dissolved in deionized water at 30 °C and stirred until the solution becomes clear. A second mixture with HCl and P123 was prepared at 30 °C stirred until clear solution. The two solutions were mixed and stirred rigorously for 30 min. A separate solution was prepared by dissolving metal precursors in ethanol and stirring approximately for 30 min. The dissolved metal solution was gently poured into the solution mixture and stirred vigorously for 30 min. TMOS, the limiting reagent for this chemical synthesis, was added dropwise into the mixture while stirring continuously for another 30 min, followed by adding TIPR dropwise stirred for another 30 min. The mixture was then stirred for another 3 h, followed by aging for 24 h at 110 °C. The aged material was dried in air for 24 h then dried in an oven at 110 °C for 24 h. This dried catalyst was calcined at 550 °C for 16 h with a heating rate of 2 °C/min to remove the surfactant. It was then cooled to room temperature at a rate of 2 °C/min.

2.3. Composite oxide supports for metal impregnation

The theoretical ratio of each oxide within the mixed oxide composite support was 50 wt%. The metal precursor salt solutions were added to the already calcined supports by incipient wet-impregnation (IWI) method. Stoichiometric molar ratios of cobalt nitrate and ruthenium chloride were mixed according to the desired loading and dissolved in water to prepare the aqueous solution. The volume of the solution used for each composite support was determined by the total pore volume of the catalyst from BET analysis. The aqueous solutions of cobalt and ruthenium salts were mixed with each composite support and stirred vigorously before drying at 90 °C, followed by calcination at 350 °C for 6 h. All the synthesized catalysts after calcination are expected to contain 10 wt% Co and 5 wt% Ru.

2.4. Catalyst Characterization

The N_2 adsorption-desorption isotherms of all catalysts were measured by the BET surface area analyzer (Model: 3Flex, Make: Micromeritics, USA) instrument at constant liquid N_2 temperature (−196 °C). The surface areas and pore size distributions were calculated by N_2 adsorption-desorption isotherm using the Brunauer-Emmett-Teller (BET) and Barrett-Joyner-Halenda (BJH) method. The X-ray diffraction was carried out using a powder X-Ray diffractometer (Model: Bruker AXS). The detection limit of the instrument was in the range of 10-80° with a step interval of 0.02° using a Cu Kα1 radiation source with a wavelength of 1.5406 Å. Peaks observed in these spectra were used to identify the catalyst metals, their oxidation state, and morphology. Temperature programmed reduction was performed using a chemisorption analyzer (Mode: 3Flex, Make: Micromeritics, USA). 0.05 g of sample material was measured and placed into a chemisorption tube on top of a covering layer of quartz wool beneath a quartz filter cap upon which the sample was placed. The sample was then placed under a 10 % H_2/Ar (1:9wt %) flow of 50 ml/min and a ramp rate of 10°C/min from room temperature to 800 °C to determine reducibility of the metal oxides. Synthesized materials were imaged using a ZEISS Auriga Focused Ion Beam Scanning Electron Microscope (FIBSEM) provided by the Joint School of Nanoscience and Nanoengineering. These images were used to draw conclusions of the average particle size, morphology and topography of each catalyst. The Transmission Electron Microscopy (TEM) was carried out by Thermo Fischer Talos (Model: F200X). The field emission system was operated at 200 kV. The decomposition temperature of polymer-templates, used in the mixed composite support preparation, was determined by Thermogravimetry and Differential scanning Calorimetry (TGA-DSC) (Model: TA instruments, New castle, DE, USA). Sample was heated to 1000 °C at a heating rate of 10°C/min. The analysis was done in presence of Air at 100 ml/min. The oxidation states of all catalysts were determined by X-ray photoelectron Spectroscopy (Model: Escalab Xi + -, Make: Thermo Scientific, West Sussex, UK).

2.5. Microreactor fabrication

3D printing technology was used to fabricate microchannel microreactors and respective cover channels as described previously [38]. Basically, they are designed by AutoCAD software is shown in our previous work [38]. The microreactor has 11 microchannels of 500 μm × 500 μm × 2.4 cm as reaction zone in between them. The stainless steel microreactor is assembled in a heating block with inlet and outlet channels which facilitates syngas to pass through it.

2.6. Catalyst loading into the microreactor

The catalyst was loaded into the microchannels of the microreactor using a PVA solution containing the catalyst and acetic acid. The microreactor was dip-coated in the PVA solution, sonicated for about 5 min and dried in air. Then the microreactor was calcined ex-situ in the presence of air at 550 °C for 6 h with heating and cooling rates of 1 °C/min to remove the acetic acid and PVA. The calcined microreactor was finally loaded into the reaction block and reduced prior to FT reactions

2.7. Catalyst activity test

FTS was carried out in a Stainless-Steel microchannel microreactor at four different temperatures (180, 210, 240 and 270 °C) and 1 atm with an H_2/CO molar ratio of 2. We maintained 12,000 h^{-1} GHSV for each reaction. The LabVIEW software was used to control the reaction parameters (temperature, flow rate and pressure). The gas flow rate was controlled by Cole-Parmer mass flow controller with 0.2 ml/min of CO and 0.4 ml/min of H_2. Nitrogen was used as a carrier gas and its flow rate was controlled by Aalborg mass flow controller within the range of 0 to 10 ml/min. The upstream and downstream pressures were monitored by pressure gauge continuously. The stream of product gases was directly fed to the GC-MS (Model: 7890B GC and 5977A MSD; Make: Agilent Technologies). Before the FTS, the catalyst loaded microreactors were reduced ex-situ in Carbolite Gero tubular furnace in presence of 10 % H_2 and Ar mixture. In order to compensate for the loss of catalyst reactivity during transfer of the microreactor into the heating block, the catalyst loaded microreactor was again reduced in-situ at 350 °C for 6 h before the start of the FTS. The reactions reached a steady state after one hour. CO conversion and hydrocarbon selectivity were calculated based on the following equations [37,38]:

Although production of CO_2 from the water gas shift reaction is important, CO_2 selectivity was not included in the calculation because the primary objective was to understand the effect of different mesoporous mixed composite oxide support and the Co, Ru metals on CO conversion and hydrocarbon selectivity [37].

3. Results and discussion

3.1. Catalyst characterization

3.1.1. N_2 adsorption–desorption isotherms

Low-temperature N_2 adsorption-desorption isotherms for three different mesoporous supports and CoRu based catalysts are shown in Fig. 1(a). The BET surface areas are shown in Table 1. The isotherms of $mSiO_2$-Al_2O_3, $mSiO_2$-TiO_2, CoRu/m-SiO_2-Al_2O_3, CoRu/m-SiO_2-TiO_2 and CoRu/m-SiO_2-TiO_2 (OP) correspond to type IV, whereas those of mAl_2O_3-TiO_2 and CoRu/Al_2O_3-TiO_2 are of Type II, according to IUPAC classification [50,51]. Isotherms of all samples have hysteresis loops of different types: $mSiO_2$-Al_2O_3 is H1 type; $mSiO_2$-TiO_2 and mAl_2O_3-TiO_2 are H_3 type; and all metal containing catalysts are H4 type [52]. Incorporation of CoRu into the supports did not affect the shape of the

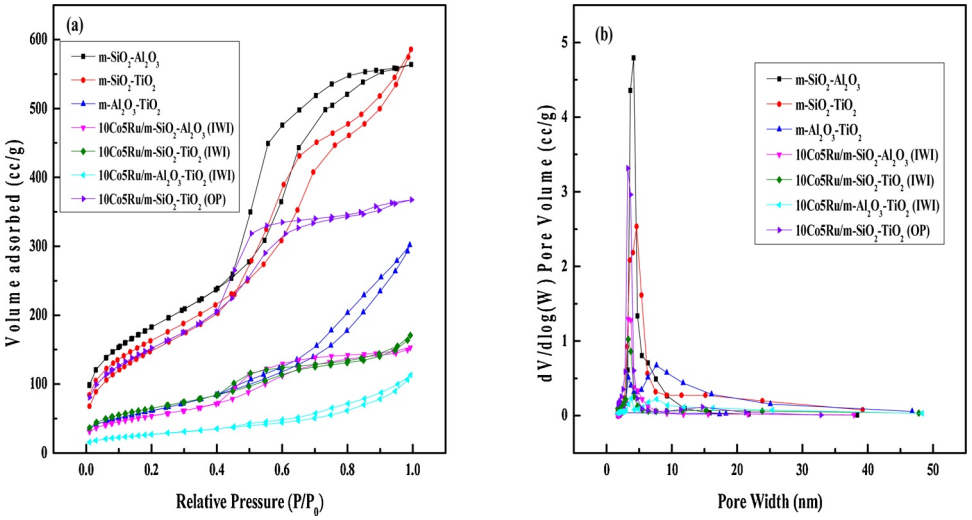

Fig. 1. (a) N_2 adsorption-desorption isotherms and (b) pore size distributions of three different mesoporous supports and CoRu-loaded catalysts.

isotherm significantly, but it changed the type of hysteresis loop. It is the result of partial filling of metal clusters into the pores of the supports, which did not substantially change the porous matrix but reduced the pore volume and the pore shapes [53]. The mesoporous SiO_2-Al_2O_3 and SiO_2-TiO_2 supports exhibited higher pore volumes and surface areas, establishing the expansion of mesopores upon introducing Al [52] and Ti into mesoporous SiO_2 framework. The capillary condensation between adsorption and desorption of N_2 occurred at liquid nitrogen temperature in the pores, producing this kind of isotherm pattern [54]. The corresponding supports and catalysts pore size distribution curves are shown in Fig. 1(b). The distribution curve shows that the pore sizes of CoRu/m-SiO_2-Al_2O_3 (IWI), CoRu/m-SiO_2-TiO_2 (IWI), CoRu/m-Al_2O_3-TiO_2 (IWI) and CoRu- m-SiO_2-TiO_2 (OP) catalysts are similar but little bit smaller than the supports (m-SiO_2-Al_2O_3, m-SiO_2-TiO_2 and m-Al_2O_3-TiO_2), indicating that pores of the supports are partially occupied by the added metal oxides. This confirmed a partial loss of the structural integrity of the mixed oxide supports upon incorporation of the metals (see the SEM image in supplementary section).

3.1.2. *Temperature programmed reduction (TPR)*

The H_2-TPR profiles of the supported CoRu based catalysts are shown in Fig. 2. TPR studies were carried out to understand the reducibility of supported CoRu particles. The reduction profiles of catalysts were obtained under the flow of 10 % H_2/Ar. Supplemental Fig. S1 shows the H_2-TPR profiles of the bare mesoporous composite oxide supports. No reduction peaks are observed for the supports. In Fig. 2, the TPR profile of CoRu/m-SiO_2-Al_2O_3 (IWI) catalyst showed the reduction peaks around 326 °C and 448 °C that correspond to formation of metallic Co via two-step reduction of Co_3O_4 crystals [Co_3O_4 + H_2 = 3CoO + H_2O and CoO + H_2 = Co + H_2O] with intermediate formation of CoO species [55,56]. The peak at 190 °C corresponds to reduction of RuO_2 to Ru° [57]. In the case of the CoRu/m-SiO_2-TiO_2

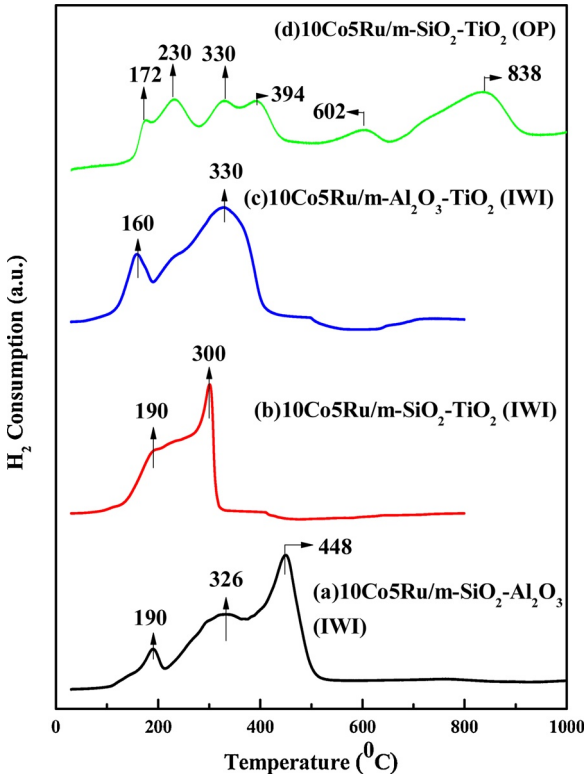

Fig. 2. H_2-TPR profiles of all composite oxides supported CoRu catalysts.

Table 1
N_2 adsorption-desorption analysis data of different mixed composite supports and catalysts.

Catalysts and support	Surface area (m^2/g)	Pore diameter (nm)	Avg. pore volume (cc/g)
m-SiO_2-Al_2O_3	654.78	5.33	0.87
m-SiO_2-TiO_2	594.02	6.08	0.90
m-Al_2O_3-TiO_2	225.85	8.26	0.46
10Co5Ru/m-SiO_2-Al_2O_3 (IWI)	192.46	4.92	0.24
10Co5Ru/m-SiO_2-TiO_2 (IWI)	230.83	4.55	0.26
10Co5Ru/m-Al_2O_3-TiO_2 (IWI)	97.80	7.11	0.17
10Co5Ru-m-SiO_2-TiO_2 (OP)	552.92	4.11	0.56

(IWI) catalyst, reduction of all metal oxides was achieved at a lower temperature (< 400 °C). The reduction for the formation of stable CoO intermediate is not clear due to overlaps of two reduction peaks. This was probably caused by the presence of Ru which lowered the reduction temperature via hydrogen spillover effect or even direct Co-Ru interactions [58–60]. The presence of Ru also possibly facilitated reduction of Co species by dissociating H_2 molecule to give active hydrogen atoms [61]. Dissociation of H_2 that leads to the hydrogen spillover effect was mainly influenced by the support characteristics, distribution of the metals, interactions between two metals, and the adsorption capacity of the catalysts [62–64]. More specifically, the spillover effect of CoRu/m-SiO_2 -TiO_2 (IWI) was due to the combined effect of high surface area (Table 1) and the relatively weaker ruthenium-support interactions observed in the XPS analysis (Table 4). This is evident in the mesoporous SiO_2-TiO_2 composite oxide support, where Ru played an important role to reduce the reduction temperature. The peak around 160 °C was attributed to reduction of RuO_2 to Ru° for the CoRu/m-Al_2O_3-TiO_2 catalyst. Another peak at about 330 °C was assigned to reduction of Co_3O_4 to Co [1]. However, a different TPR profile was obtained for CoRu-m-SiO_2-TiO_2 (OP) catalyst. Several reduction steps occurred at a higher temperature suggesting that this support has a strong interaction with the Co species. The two peaks around 602 °C and 838 °C are attributed to the reduction of cobalt titanates and silicates mixed metal oxides [65]. Four distinct reduction peaks were observed at temperature below 400 °C. These peaks are basically attributed to the reduction of RuO_2 and Co_3O_4. The presence of Ru lowered the reduction temperature of cobalt [66]. Thus, the variation of mesoporous support and catalyst preparation methods play an important role in the reduction of CoRu species.

Table 2 shows the H_2 consumption of different catalysts during TPR analysis. The highest H_2 consumption was observed for CoRu/m-SiO_2-Al_2O_3 (IWI) catalyst and it suggests the presence of maximum amount of reducible species. In contrast, the lowest H_2 consumption was observed for CoRu-SiO_2-TiO_2 (OP) catalyst. The catalyst contains a greater number of non-reducible species or in other words very difficult to reduce. Table 2 also shows the reduction degree (%) of different catalysts. The reducibility of the Co based catalyst has been observed in the temperature range of 150 to 400 °C [67]. This temperature range is used because it covers most of the reaction temperatures used for FT synthesis. Based on our TPR results shown in Table 2, the highest reduction degree is observed for CoRu/m-SiO_2-TiO_2 (IWI) catalyst. The main reduction peak at 448 °C is observed for CoRu/m-SiO_2-Al_2O_3 (IWI) catalyst. This temperature is outside the reduction temperature range (150 to 400 °C). So, the reduction degree (%) of CoRu/m-SiO_2-Al_2O_3 (IWI) catalyst is low.

3.1.3. X-ray diffraction (XRD)

XRD analysis was carried out to ascertain the metal oxide crystal phases present in the catalysts. Fig. 3 (A) exhibits the low angle XRD patterns of different mesoporous oxide supports. In the case of m-SiO_2-Al_2O_3 support, the well-resolved peak at $2\theta = 1.4^\circ$ is observed. This is the characteristics of mesoporous material [plane (1 1 0)] with 2D-hexagonal structure [68]. However, for m-SiO_2-TiO_2 prepared by one-pot procedure, no such peak is observed. Low angle XRD of m-Al_2O_3-TiO_2 support was not performed because this sample does not contain ordered pores as observed in mesoporous silica. Fig. 3 (B) shows the XRD patterns of different catalysts. The diffraction peaks at various 2θ angles such as 19.05°, 31.27°, 36.78°, 44.89°, 59.21° and 65.14° correspond to Co_3O_4 with cubic structure, indicating that Co_3O_4 is the primary crystalline cobalt species [69,70]. Some weak peaks at $2\theta = 28.31^\circ$ and 54.29° correspond to RuO_2 with tetragonal structure [71,72]. The weak intensity peaks of RuO_2 are possibly observed due to interaction of Ru with Co species. This appears to be consistent with the TPR results. The anatase phase of TiO_2 is observed at a 2θ angle of 25.36° and 48.60° for only CoRu/m-SiO_2-TiO_2 (IWI) [73]. However, in the case of CoRu-m-SiO_2-TiO_2 (OP) catalyst, only one peak for anatase phase of TiO_2 at 25.36° and a very weak intensity peak of Co_3O_4 at 36.78° are observed. This could be due to the fact that the one pot procedure produces ordered *cage-like* frameworks (see isotherms in Section 3.1.1) which may tend to shield the metal oxides from the incident X-rays. Table 3 shows the average crystal size of different crystals of Co_3O_4, RuO_2 and TiO_2. Modified Scherrer equation, as described elsewhere [74], is used to determine the average crystal size. The average crystal sizes of CoRu/m-SiO_2-Al_2O_3 (IWI), CoRu/m-SiO_2-TiO_2 (IWI), CoRu/m-Al_2O_3-TiO_2 (IWI) and CoRu-m-SiO_2-TiO_2 (OP) catalysts are shown in Table 3. The average crystal sizes of Co_3O_4 and RuO_2 for CoRu/m-SiO_2-Al_2O_3 (IWI) and CoRu/m-SiO_2-TiO_2 (IWI) are almost same. This suggests the uniform distribution of metal particles over the large surface areas of the supports. In the case of CoRu/m-Al_2O_3-TiO_2 (IWI) and CoRu-SiO_2-TiO_2 (OP) catalysts, the average crystal size is quite large. It suggests that the metal oxide has a weak interaction with the support, which can easily agglomerate resulting in a poor/less uniform distribution.

In general, the crystal sizes of noble metals are known to be smaller than that of transition elements; it depends on structural rearrangements (e.g. substitutional, interstitial, and intermetallic alloy formation) in the presence of other metals. The first possibility is that the relatively larger number of Co species outcompeted the Ru oxides for the binding sites of the support which could lead to agglomeration of the Ru oxide crystallites. The 6.5 nm crystal size of the TiO_2 anatase phase is very small compared to the other metal oxides. This suggests a strong interaction between SiO_2 and TiO_2. The implication is that the addition of SiO_2 to TiO_2 stabilized the anatase phase which hindered the chain growth and hence agglomeration of the TiO_2 crystallites [75].

3.1.4. Transmission electron microscopy (TEM)

The TEM images of Co-Ru catalysts with different mesoporous mixed composite supports prepared by IWI and that of CoRuSiO_2-TiO_2 prepared by one-pot (OP) are shown in Fig. 4. The dark spots correspond to the metal oxides formed over the mesoporous support. These micrographs do not reveal information about distinct particle distribution of Ru-Co mixed oxide phases. However, the images of calcined IWI catalysts exhibited some agglomeration of metal oxides over different supports [See also the SEM images in Supplemental Fig. S4]. The metal oxides can block partially or completely the pores of the support leading to a partial structural degradation of the mixed oxide supports

Table 2
The H_2 consumption and reduction degree at 150–400 °C for the prepared catalysts.

Catalysts	H_2 Consumption (μmol/g)[a]	Reduction degree (%)[b]
10Co5Ru/m-SiO_2-Al_2O_3 (IWI)	324.09	47.74
10Co5Ru/m-SiO_2-TiO_2 (IWI)	273.01	95.27
10Co5Ru/m-Al_2O_3-TiO_2 (IWI)	271.48	92.53
10Co5Ru-m-SiO_2-TiO_2 (OP)	153.23	34.46

[a] The H_2 consumption (μmol/g) was defined as the measured amount of H_2 consumption in TPR peak /theoretical H_2 consumption (μmol H_2/g) × 100.

[b] The degree of reduction (%) was defined according to the literature [67] as the measured amount of H_2 consumption between 150-400 °C in TPR peak /theoretical H_2 consumption (μmol H_2/g) × 100.

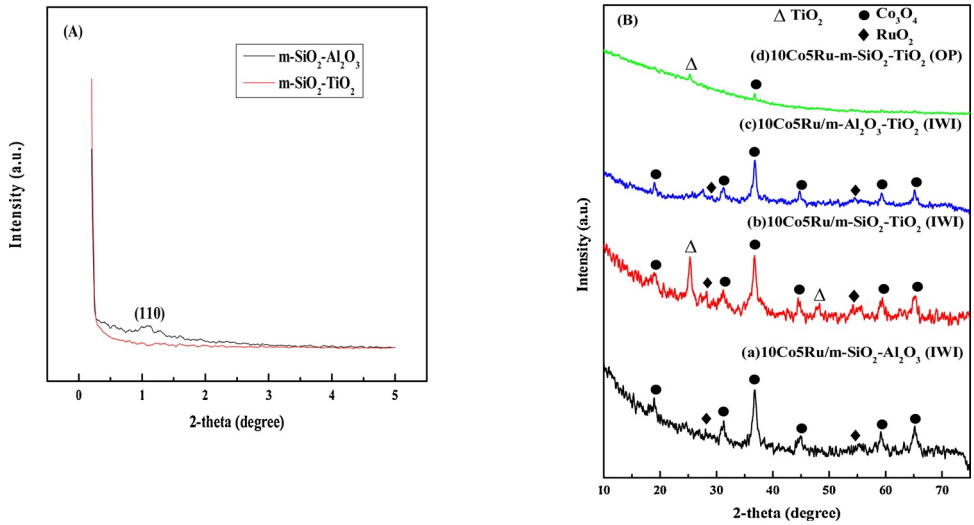

Fig. 3. XRD analyses: (A) Low angle XRD of mesoporous composite support; (B) WAXRD of different mesoporous composite oxides supported CoRu based catalysts.

Table 3
Crystal size calculation* based on XRD data.

Catalysts	Crystal Size (nm)		
	Co_3O_4	RuO_2	TiO_2
10Co5Ru/m-SiO_2-Al_2O_3 (IWI)	21.37	88.54	–
10Co5Ru/m-SiO_2-TiO_2 (IWI)	17.98	87.24	6.53
10Co5Ru/m-Al_2O_3-TiO_2 (IWI)	23.51	38.66	–
10Co5Ru-m-SiO_2-TiO_2 (OP)	40.42	–	38.68

* Using Modified Scherrer equation [74].

Table 4
The transition states of cobalt and ruthenium in all the mesoporous composite oxides supports.

Catalyst	Co $2p_{1/2}$ (eV)	Co $2p_{3/2}$ (eV)	Ru $3d_{3/2}$ (eV)
10Co5Ru /SiO_2-Al_2O_3	796.03	781.05	284.3
10Co5Ru /SiO_2-TiO_2	795.86	780.86	284.1
10Co5Ru /Al_2O_3 -TiO_2	795.94	780.69	284.6

and hence a decrease in the surface area. The decrease in surface area caused by incorporation of metal oxides as well as the partial loss/degradation of the support structure are consistent with the results of N_2 adsorption-desorption isotherms. In the case of calcined OP catalyst, the TEM image shows that metal oxides were well distributed over the support. The agglomerated metal oxides particles on the support could decrease scattering contrast between the pore and the walls of the support [76,77].

3.1.5. Thermogravimetry and differential scanning calorimetry (TGA-DSC)

Fig. 5 shows the TGA-DSC profiles of as-synthesized (not calcined) mixed oxide mesoporous supports. The first weight loss below 190 °C is due to the removal of volatile solvents used for the catalyst preparation and water/moisture adsorbed on the support surfaces. The second weight loss between 190 °C and 240 °C were caused by the decomposition of the pluronic acid (P123) template used for synthesis. The third weight loss from 250 °C to 380 °C was due to the decomposition of the surfactant-CTAB [78]. The differences in the weight losses (peak heights) of the P123 and CTAB are due to their different molar concentrations used for the synthesis in Section 2.2. In the case of Fig. 6b, the additional exothermic weight loss from 400 °C to 500 °C could be attributed to phase transition of amorphous TiO_2 to the crystalline anatase polymorph similar to observations made by Deshmane et al. [79]. This phase transition is consistent with our XRD diffraction patterns described in Section 3.1.3 which showed that only the SiO_2-TiO_2 (IWI) composite matrix possessed a substantial proportion of the TiO_2 anatase crystal structure. No change in weight loss was observed above 500 °C, indicating that all the composite oxides were thermally stable.

3.1.6. X-ray photoelectron spectroscopy (XPS)

The chemical states of cobalt and ruthenium in mixed oxide supports were determined from XPS studies. The Fig. S3 shows the spectra for the mixed oxide supports Si 2p centered at 153 eV, Ti centered at 464 eV and O 1s at 531 eV which confirms the presence of two supports in the catalyst. Table 4 lists the position of transition states of cobalt and ruthenium in all the composite supports. In Table 4, the difference in the binding energies of Co 2p spectra for Co $2p_{3/2}$ and Co $2p_{1/2}$ peak intensities indicate interaction of Co metal with different types of support. This suggests that the microstates of Co electronic transitions are also dependent on the type of support. The results clearly show that the interaction is greatly dependent on the type of the composite support. This is also consistent with the TPR results (Section 3.1.2) showing different reduction temperatures for Co metal when the support is changed. The XPS spectra for Co 2p and Ru 3d are shown in Fig. 6a and b, respectively. The deconvolution of Co 2p in Co $2P_{1/2}$ and $Co2p_{3/2}$ with a satellite peak is shown for all samples indicating the presence of two Co-oxidation states in Co_3O_4 [80]. The peaks in CoRu/SiO_2-Al_2O_3 are shifted to higher binding energies when compared to the other two catalysts showing the strong metal-support interactions in SiO_2-Al_2O_3 support [38]. The presence of RuO_2 and hence Ru^{4+} oxidation state is confirmed by Ru 3d spectra with a binding energy centered around 284 eV. In the case of cobalt catalysts, the binding energy suggests that both Co^{2+} and Co^{3+} species are present in the catalyst framework [81]. This is also consistent with the TPR profiles for the reduction of metals in three different supports. It was also noticed that XPS spectra for Ru exists in Ru 3d3/2 transition state which is shown in Fig. 6b. However, no significant differences in binding energies for Ru were observed when compared to Co 2p spectra in different mesoporous supports. It is conspicuous that the XPS intensities varied among the catalysts. Usually in XPS, the peak intensity is a measure of how much of each element is present at the outermost surface of the material. Thus, differences in metal-support interactions which affect the degree of exposure and distribution of the active sites impacts the spectral intensities significantly. In CoRu-Al_2O_3-TiO_2 sample, the peak intensities of Co and Ru are less compared to the other catalysts indicating that very small amount of the metals are present on the surface of the material. It can therefore be speculated that most of the Co and

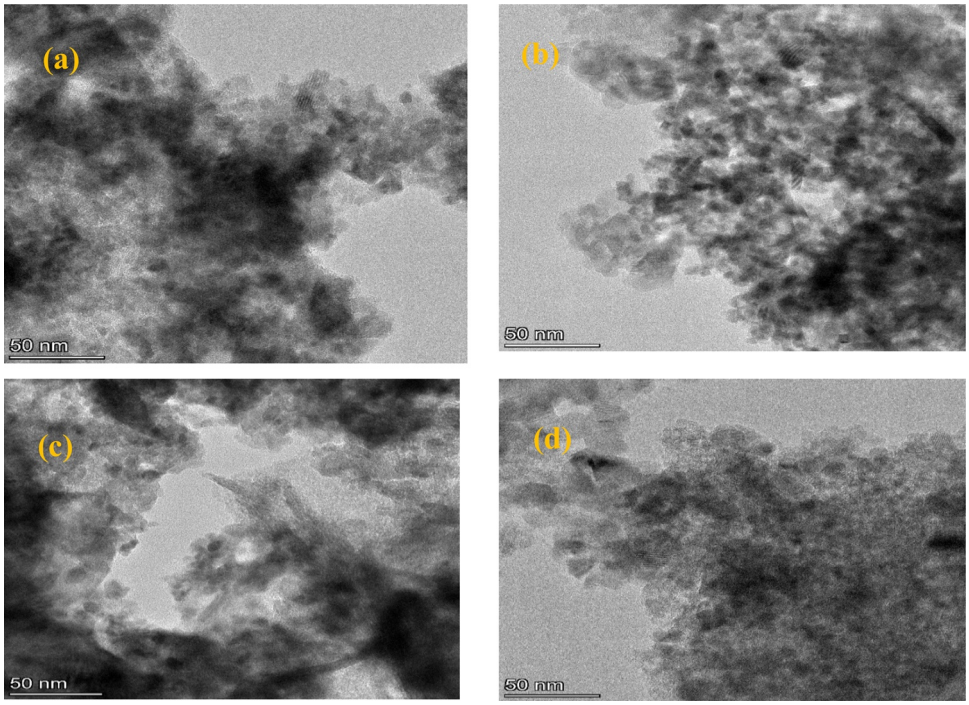

Fig. 4. TEM images of Co-Ru catalysts with different mesoporous mixed composite supports prepared by incipient wetness impregnation (IWI) and one-pot (OP) methods: (a) 10Co5Ru/m-Al_2O_3-TiO_2 (IWI); (b) 10Co5Ru/m-SiO_2-TiO_2 (IWI); (c) 10Co5Ru/m-SiO_2-Al_2O_3 (IWI); (d) 10Co5Ru-m-SiO_2-TiO_2 (OP).

Ru particles may have been entrapped within the mesoporous framework, shielding them from the incident X-rays.

3.2. Fischer–Tropsch synthesis (FTS)

3.2.1. m- SiO_2-Al_2O_3 (IWI) catalysts

The effect of reaction temperature on different mesoporous composite oxide supported CoRu catalysts activity was investigated to know the optimum reaction temperature for CO conversion and hydrocarbon selectivity of each catalyst. The reactions were carried out at four different temperatures (180, 210, 240 and 270 °C) and at 1 atm with a H_2/CO molar ratio of 2. The FT reaction mainly produced methane, ethane and propane, which are in reasonable agreement with previous work on FT synthesis at 1 atm [82].

Fig. 7 shows the effect of temperature on CoRu/m-SiO_2-Al_2O_3 catalyst activity in terms of CO conversion and selectivity towards hydrocarbons. CO conversion increased initially up to 210 °C, then it decreased at higher temperature (> 210 °C). Methane, CH_4, selectivity was almost constant throughout the experimental range of temperature. CO conversion decreased more at temperatures greater than 210 °C because of reverse water gas shift reaction ($CO_2 + H_2 = CO + H_2O$, $\Delta H_{298} = 41$ kJ/mol) that is thermodynamically feasible at higher temperatures. FT synthesis shows propane formation starting at 210 °C, while ethane and propane selectivity were almost constant throughout the temperature range up to 210 °C. The highest CO conversion was 74.7 % at 210 °C.

3.2.2. m-Al_2O_3-TiO_2 (IWI) catalysts

As shown in Fig. 8 for CoRu/m-Al_2O_3-TiO_2 (IWI) catalyst, CO conversion increased up to 210 °C, then it decreased at higher temperature. Consequently, methane selectivity decreased initially up to 210 °C, then it increased at higher temperature. The formation of methane at higher temperature revealed that catalyst was active for methanation reaction. Ethane selectivity increased up to 210 °C, then it decreased at higher temperature. Highest CO conversion and ethane selectivity were 61.98 % and 14.84 %, respectively at 210 °C.

3.2.3. m-SiO_2-TiO_2 (IWI) catalysts

Fig. 9 shows the effect of reaction temperature on CoRu/m-SiO_2-TiO_2 (IWI) catalyst activity in terms of CO conversion and product selectivity. CO conversion increased initially up to 210 °C, then decreased at higher temperature. At higher temperature, the catalyst was active for reverse water gas shift reaction. Methane selectivity was constant throughout the temperature range. Initially at 180 °C, the formation of ethane was more. However, when the temperature is increased, the ethane selectivity decreased a little, then it increased again. No propane was observed at 180 °C. Propane started to form around 210 °C. Highest CO conversion of 68.59 % was observed at 210 °C. In conclusion, CoRu/m-SiO_2-TiO_2 (IWI) catalyst showed promising activity in terms of CO conversion when compared to the catalysts impregnated on other mixed mesoporous supports. Interestingly, TPR study showed that this catalyst was completely reduced below 400 °C (Figure 2). So, we compare CoRu/m-SiO_2-TiO_2 (IWI) with CoRu/m-SiO_2-TiO_2 (OP) catalyst for FT studies to investigate the effect of preparation procedure on the catalyst's activity (next below).

3.2.4. m-SiO_2-TiO_2 (OP) catalysts

Fig. 10 shows the effect of reaction temperature on CoRu/m-SiO_2-TiO_2 (OP) catalyst activity in terms of CO conversion and product selectivity. CO conversion increased with the increase of reaction temperature up to 210 °C, then decreased. This was possibly due to reverse water gas shift reaction at higher temperature. Methane and ethane selectivity were almost constant throughout the temperature range. Highest CO conversion of 47.99 % was observed at 210 °C. This catalyst showed lower activity than the catalyst prepared by IWI method. This is likely due to a smaller number of reducible Co and Ru metals in the catalyst prepared by one-pot method and consistent with our TPR studies (Figure 2) where the reduction peaks at higher temperature are observed. As the metals in the sample prepared by OP method involved stronger interaction with the mesoporous support, it was difficult to reduce them with H_2. t. Thus, the catalyst support and the method of preparation play an important role in catalyst activity studies.

In all cases, maximum amount of methane was produced when compared to other hydrocarbons. This is most likely due to the fact that

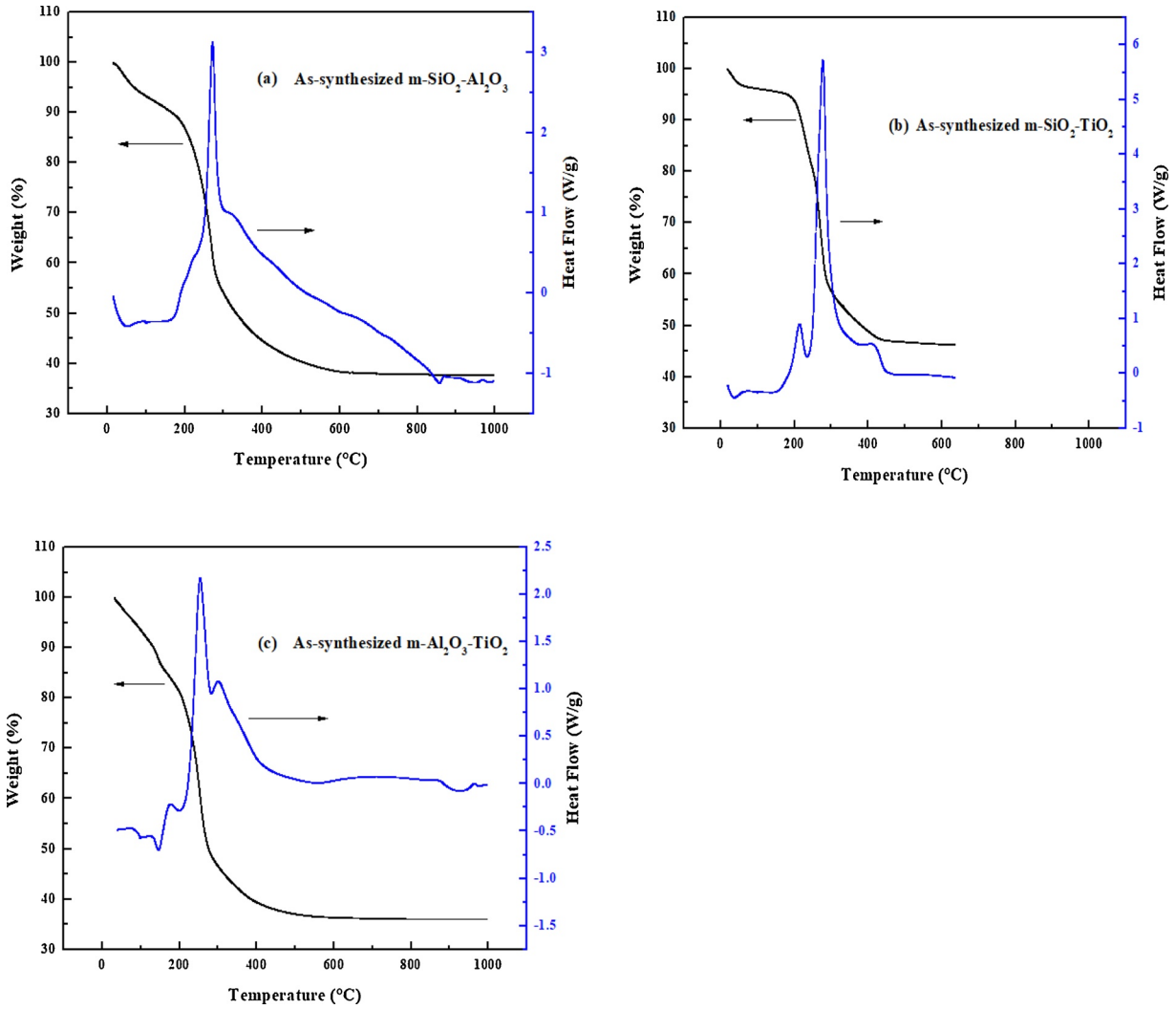

Fig. 5. TGA-DSC profiles of: (a) as-synthesized m-SiO_2-Al_2O_3; (b) as-synthesized m-SiO_2-TiO_2; (c) as-synthesized m-Al_2O_3-TiO_2 supports.

FT reactions were carried out at atmospheric pressure. The high selectivity to methane might be explained by the Anderson-Schulz-Flory mechanism [83,84]. The methane formation was possible at several metal active sites during hydrogenation but not active for FT synthesis. For Co based catalyst, methane formation mainly depends on partial pressure of CO, H_2, H_2O and temperature [85]. So, increasing temperature as well as partial pressure of H_2 could help to suppress the formation of methane [86]. Formation of large amount of methane relative to ethane and propane indicates very limited/low polymerization on the active sites. This suggests that the rate of initial surface carbide formation (via CO decomposition) is faster than the rate of formation of hydrocarbon chain extenders (—CH_2—CH_2 groups)

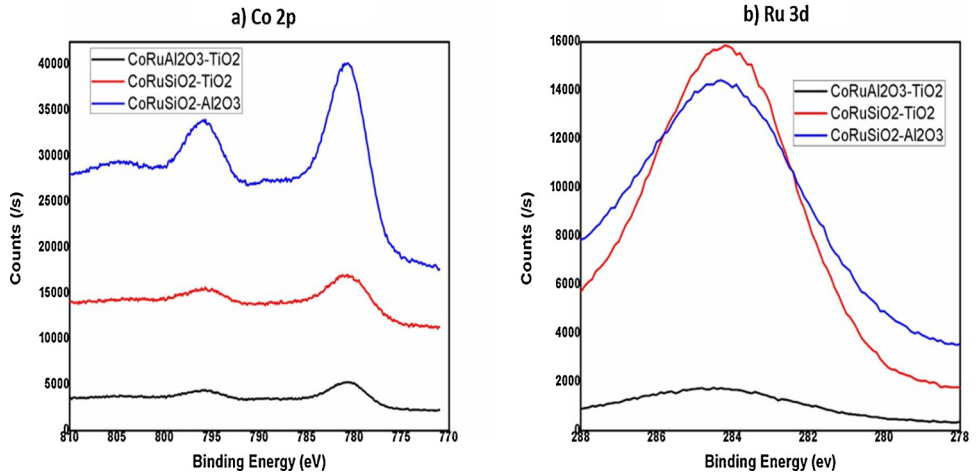

Fig. 6. XPS spectra of (a) Co 2p (b) Ru 3d of all CoRu bimetallic catalysts.

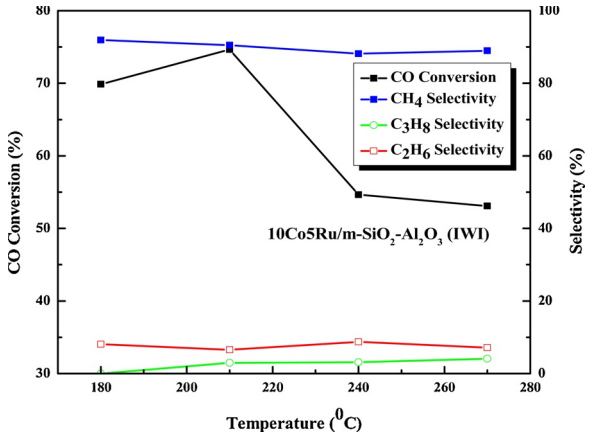

Fig. 7. Effect of temperature on CO conversion and product selectivity in FT synthesis using 10Co5Ru/m-SiO_2-Al_2O_3 (IWI) catalyst (Conditions: H_2/CO = 2, 1 atm, 12000 h^{-1} GHSV).

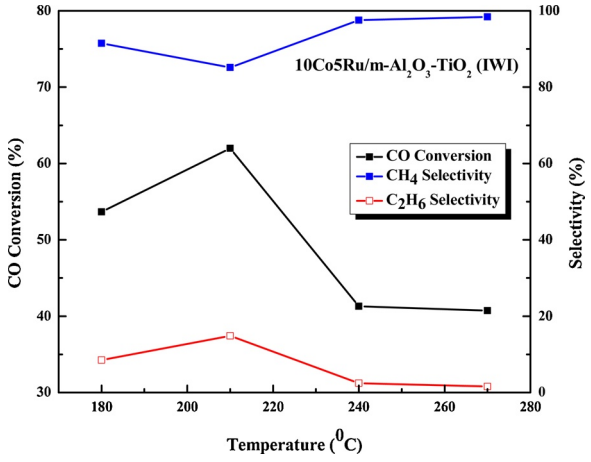

Fig. 8. Effect of temperature on CO conversion and product selectivity in FT synthesis using 10Co5Ru/m-Al_2O_3-TiO_2 (IWI) catalyst (Conditions: H_2/CO = 2, 1 atm, 12000 h^{-1} GHSV).

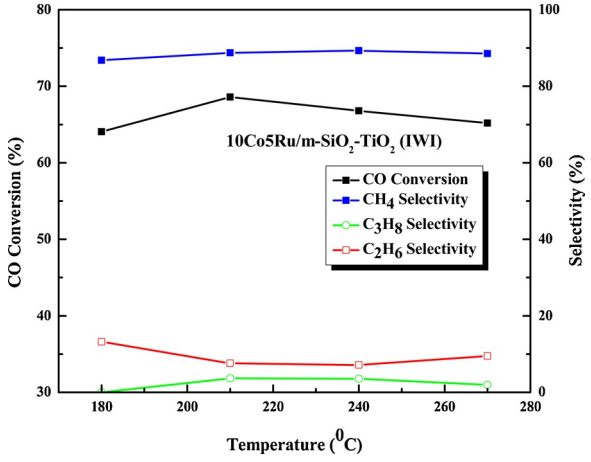

Fig. 9. Effect of temperature on CO conversion and product selectivity in FT synthesis using 10Co5Ru/m-SiO_2-TiO_2 (IWI) catalyst (Conditions: H_2/CO = 2, 1 atm, 12000 h^{-1} GHSV).

[87]. Thus, carbidization causes clogging of metal active sites with carbon deposits that ultimately disrupts polymerization to higher hydrocarbons. Therefore, the increase in methane selectivity with the decrease in selectivity towards ethane and propane was possibly caused

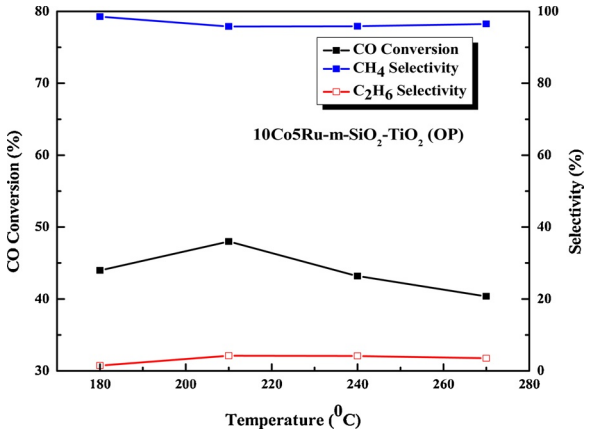

Fig. 10. Effect of temperature on CO conversion and product selectivity in FT synthesis using 10Co5Ru-m-SiO_2-TiO_2 (OP) catalyst (Conditions: H_2/CO = 2, 1 atm, 12000 h^{-1} GHSV).

by the deposition of carbon on the catalyst active sites via CO decomposition. Evidently, retardation or disruption of the chain growth prevents formation of higher hydrocarbons [87,88] at 1 atm due to coke formation. In this study, product formation mainly depended on different mesoporous support. Propane was observed for mesoporous SiO_2-Al_2O_3 and SiO_2-TiO_2 supported IWI catalysts. Thermodynamically, the lower olefins are produced in FT synthesis at higher pressure [89,90]. However, this work was done at 1 atm. So, we found only lower alkanes.

3.3. Continuous time-on-stream behavior of all catalysts

In order to know the time-on-stream behavior or stability of the catalysts, all the catalysts were tested for 60 h at 210 °C, 1 atm with H_2 to CO molar ratio of 2. Fig. 11 shows the stability study of all catalysts based on CO conversion. After initial drop on CO conversion, all the catalysts showed good stability during 60 h operation. Highest CO conversion, ~75 %,was achieved with 10Co5Ru/m-SiO_2-TiO_2 (IWI) catalyst. Lowest CO conversion (53 %) was observed with 10Co5Ru-SiO_2-TiO_2 (OP) catalyst. This result suggests that the method for the catalyst preparation played an important role on stability studies. For 10Co5Ru/m-SiO_2-Al_2O_3 (IWI) catalyst, ~65 % CO conversion was obtained. In the case of 10Co5Ru/m-Al_2O_3-TiO_2 catalyst, 55 % CO conversion was achieved during 60 h stability studies. Thus, the type of support has a great influence on the deactivation rate of the catalyst during FT synthesis [86]. Iglesia et al. reported that the type of support

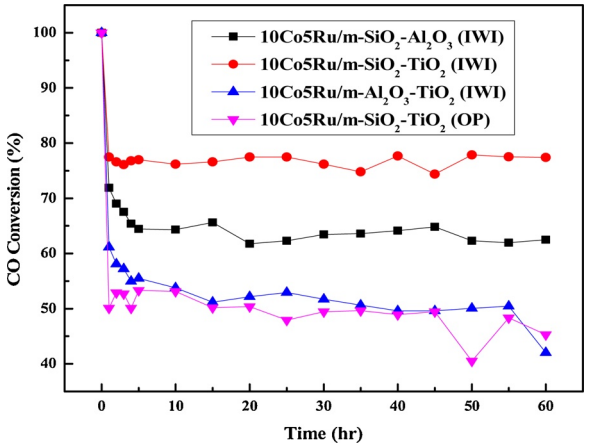

Fig. 11. Time-on-Stream behavior of all catalysts (Conditions: H_2/CO = 2, 210 °C, 1 atm, 12000 h^{-1} GHSV).

Table 5
Carbon content (wt.%) based on temperature range of 200 to 600 °C of all spent catalysts.

Catalyst	Carbon content (wt.%)
Spent 10Co5Ru/m-SiO_2-Al_2O_3 (IWI)	0.61
Spent 10Co5Ru/m-SiO_2-TiO_2 (IWI)	3.44
Spent 10Co5Ru/m-Al_2O_3-TiO_2 (IWI)	2.85
Spent 10Co5Ru-m-SiO_2-TiO_2 (OP)	2.24

can be utilized to enhance the stability of the catalyst to resist deactivation [4]. In summary, the stability and ability of the catalysts to withstand deactivation were observed in the order: 10Co5Ru/m-SiO_2-TiO_2 (IWI) > 10Co5Ru/m-SiO_2-Al_2O_3 (IWI) > 10Co5Ru/m-Al_2O_3-TiO_2 (IWI) > 10Co5Ru-m-SiO_2-TiO_2 (OP).

3.4. FT studies with catalyst supports only

In order to know the negative reaction control of the FT synthesis, reactions were also carried out with three different mesoporous composite supports. Fig. S5 shows CO conversion on the bare supports at 210 °C and 1 atm with H_2/CO molar ratio of 2. No hydrocarbon formation and CO conversion were observed with the bare catalyst supports indicating that the supports did not influence the hydrocarbon product distribution.

3.4.1. Characterization of spent catalysts

The spent catalysts were examined by temperature programmed (TPO-DSC) carbon oxidation in air and XRD analysis to ascertain the possible causes in the decline of the catalyst activity over time. Table 5 compares percent carbon deposition of the catalyst after continuous 60 h on-stream. The TGA-DSC thermal profiles of the spent catalysts are shown in supplemental Fig. S2.

Interestingly, there was no linear correlation between the carbon deposition and loss of catalyst activity after 60 h. Based on the amount of carbon deposited on the active sites, 10Co5Ru/m-SiO_2-Al_2O_3 (IWI) catalyst should have shown the highest activity and long-term stability. However, 10Co5Ru/m-SiO_2-TiO_2 (IWI) catalyst which had about 6 times as much coking compared to the former showed the highest long-term stability. The trend suggests that although coking was one of the potential causes of deactivation, other factors such as method of preparation, composition of mixed oxide support, oxidation, sintering, support degradation and attrition also played a role. Under our experimental conditions, we think the dominant effect of the stability of mixed oxide support outweighed the coke deactivation effect. Another factor could be the relative ease of reducibility of 10Co5Ru/m-SiO_2-TiO_2 (IWI) catalyst (i.e. below 400 °C) as discussed in Section 3.1.2.

Fig. 12 shows the XRD pattern of all spent catalysts. The crystal structures changed permanently, and formation of an amorphous structure is observed. The peak intensities of Co_3O_4, RuO_2 and TiO_2 crystals are also reduced. The cubic face-centered structure of carbon (JCPDS 81-2220) peaks are found in the spent catalysts. This result confirmed that carbon was deposited on the catalyst surface during the reaction. Table 6 shows the crystal size of all metal oxides after the FT reactions. The crystal size is quite reduced in the spent catalysts.

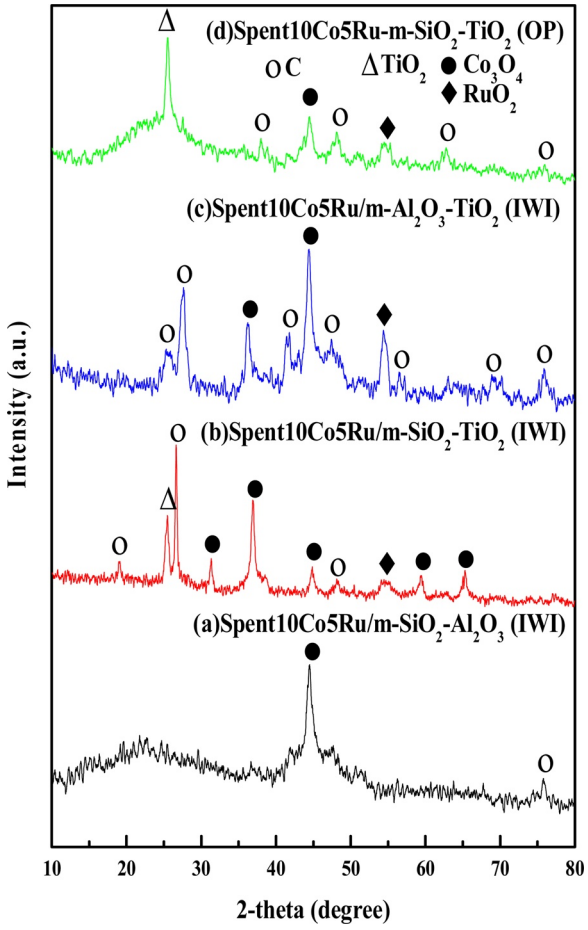

Fig. 12. XRD of spent CoRu catalysts on different mesoporous composite oxides supports.

Table 6
Crystal size* calculated from XRD data.

Catalysts	Crystal size (nm)		
	Co_3O_4	RuO_2	TiO_2
Spent 10Co5Ru/m-SiO_2-Al_2O_3 (IWI)	9.12	–	–
Spent 10Co5Ru/m-SiO_2-TiO_2 (IWI)	17.76	5.88	14.04
Spent 10Co5Ru/m-Al_2O_3-TiO_2 (IWI)	12.6	9.71	–
Spent 10Co5Ru-m-SiO_2-TiO_2 (OP)	14.08	6.08	16.98

* Using Modified Scherrer equation [74].

4. Conclusions

Stainless steel microchannel microreactors prepared using 3D-printed technology were used for FT synthesis using three different mesoporous composite oxides supported CoRu catalysts. The catalysts were coated in the microchannels of the microreactors. Catalysts were prepared using incipient wet-impregnation and one-pot hydrothermal synthesis methods. Very different physicochemical properties were observed for 10Co5Ru/m-SiO_2-Al_2O_3 (IWI), 10Co5Ru/m-SiO_2-TiO_2 (IWI), 10Co5Ru/m- Al_2O_3-TiO_2 (IWI), and 10Co5Ru-m-SiO_2-TiO_2 (OP) catalysts. The BET results showed that catalyst surface areas decreased upon impregnation of metals on the mixed oxide supports. Co_3O_4 and RuO_2 crystals in the catalysts were observed by XRD studies. Variation in reduction temperature due to different mesoporous composite oxide support-metal interaction was identified by H_2-TPR analysis. The catalyst preparation method also affected the reduction temperature of metal oxides. Among all catalysts studied, CoRu/m-SiO_2-TiO_2 (IWI) catalyst showed promising activity for FT synthesis. Although coking is a potential cause of deactivation, other factors such as method of preparation, oxidation, composition of mixed oxide support, sintering, support degradation and attrition also played a role in the stability of the catalysts.

CRediT authorship contribution statement

S. Bepari: Conceptualization, Data curation, Investigation, Writing -

original draft, Software. **Xin Li:** Data curation, Formal analysis, Resources. **R. Abrokwah:** Methodology, Supervision, Writing - review & editing. **N. Mohammad:** Methodology, Data curation, Formal analysis. **M. Arslan:** Visualization. **D. Kuila:** Conceptualization, Writing - review & editing.

Declaration of Competing Interest

The authors declare that they have no known competing financial interests or personal relationships that could have appeared to influence the work reported in this paper.

Acknowledgements

This work is performed at North Carolina A&T State University and Joint School of Nanoscience and Nanoengineering, a member of the Southeastern Nanotechnology Infrastructure Corridor (SENIC) and National Nanotechnology Coordinated Infrastructure (NNCI), which is supported by the National Science Foundation (Grant ECCS-1542174). The authors acknowledge the funding received from National Science Foundation, NSF CREST (#260326) and University of North Carolina, Research Opportunity Initiative, UNC-ROI (#110092). The authors also gratefully acknowledge the help from Dr. Kristen Dellinger for XPS studies and Dr. Cynthia S. Day of Wake Forest University, North Carolina, USA for XRD studies of the spent catalysts. We thank Prof. Moti Herskowitz of Ben-Gurion University of the Negev, Israel, for useful discussions.

References

[1] Y.S. Noh, K.-Y. Lee, D.J. Moon, Catal. Today (2019), https://doi.org/10.1016/j.cattod.2019.08.035.
[2] F. Bertella, P. Concepcion, A. Martinez, Catal. Today 289 (2017) 181.
[3] O.A. Kungurova, A.A. Khassin, S.V. Cherepanova, A.A. Saraev, V.V. Kaichev, N.V. Shtertser, G.K. Chermashentseva, E.Y. Gerasimov, E.A. Paukshtis, O.V. Vodyankina, T.P. Minyukova, G. A-J, Appl. Catal. A Gen. 539 (2017) 48.
[4] E. Iglesia, Appl. Catal. A Gen. 161 (1997) 59.
[5] M.E. Dry, Catal. Today 71 (2002) 227.
[6] E. Rytter, N.E. Tsakoumis, A. Holmen, Catal. Today 261 (2016) 3.
[7] A.Y. Khodakov, W. Chu, P. Fongarland, Chem. Rev. 107 (2007) 1692.
[8] W.M. Chen, Y.J. Ding, D.H. Jiang, Z.D. Pan, H.Y. Luo, Catal. Lett. 104 (2005) 177.
[9] D.H. Jiang, Y.J. Ding, Z.D. Pan, W.M. Chen, H.Y. Luo, Catal. Lett. 121 (2008) 241.
[10] X.H. Mo, J. Gao, N. Umnajkaseam, J.G. Goodwin Jr., J. Catal. 267 (2009) 167.
[11] S.C. Chuang, J.G. Goodwin Jr., I. Wender, J. Catal. 95 (1985) 435.
[12] A. Erdohelyi, F. Solymosi, J. Catal. 84 (1983) 446.
[13] K. Shimura, T. Miyazawa, T. Hanaoka, S. Hirata, J. Mol. Catal. A Chem. 394 (2012) 22.
[14] S. Mandal, S. Maity, P.K. Gupta, A. Mahato, P. Bhanja, G. Sahu, Appl. Catal. A Gen. 557 (2018) 55.
[15] R. Oukaci, A.H. Singleton, J.G. Goodwin Jr., Appl. Catal. A Gen. 186 (1999) 129.
[16] A.Y. Khodakov, Catal. Today 144 (2009) 251.
[17] A.Y. Khodakov, W. Chu, P. Fongarland, Chem. Rev. 107 (2007) 1692.
[18] B.Y.F. Morales, B.M. Weckhuysen, J.J. Spivey, K.M. Dooley (Eds.), Catalysis, RSC Publishing, 2006, pp. 1–40.
[19] E. Rytter, N.E. Tsakoumis, A. Holmen, Catal. Today 261 (2016) 3.
[20] T. Jermwongratanachai, G. Jacobs, W.D. Shafer, V.R.R. Pendyala, W. Ma, M.K. Gnanamani, S. Hopps, G.A. Thomas, B. Kitiyanan, S. Khalid, B.H. Davis, Catal. Today 228 (2014) 15.
[21] K. Shimura, T. Miyazawa, T. Hanaoka, S. Hirata, Appl. Catal. A Gen. 494 (2015) 1.
[22] O.L. Eliseev, M.V. Tsapkina, O.S. Dement'eva, P.E. Davydov, A.V. Kazakov, A.L. Lapidus, Kinet. Catal. 54 (2013) 207.
[23] H. Ming, B.G. Baker, M. Jasieniak, Appl. Catal. A Gen. 381 (2010) 216.
[24] J.H. Den Otter, S.R. Nijveld, K.P. De Jong, ACS Catal. 6 (2016) 1616.
[25] J. Cheng, P. Hu, P. Ellis, S. French, G. Kelly, C.M. Lok, J. Catal. 257 (2008) 221.
[26] V. Vosoughi, A.K. Dalai, N. Abatzoglou, Y. Hu, Appl. Catal. A Gen 547 (2017) 155.
[27] M. Sarkari, F. Fazlollahi, H. Ajamein, H. Atashi, W.C. Hecker, L.L. Baxter, Fuel Process Technol. 127 (2014) 163.
[28] F.G. Botes, J.W. Niemantsverdriet, J. van de Loosdrecht, Catal. Today 215 (2013) 112.
[29] S. Chambrey, P. Fongarland, H. Karaca, S. Piche, A. Griboval-Constant, D. Schweich, F. Luck, S. Savin, A.Y. Khodakav, Catal. Today 171 (2011) 201.
[30] D.A. Wood, C. Nwaoha, B.F. Towler, J. Nat. Gas. Sci. Eng. 9 (2012) 196.
[31] S.R. Deshmukh, A.L.Y. Tonkovich, K.T. Jarosch, L. Schrader, S.P. Fitzgerald, D.R. Kilanowski, J.J. Lerou, T.J. Mazanec, Ind. Eng. Chem. Res. 49 (2010) 10883.
[32] L.C. Almeida, O. Sanz, J. Dolhaberriague, S. Yunes, M. Montes, Fuel 110 (2013) 171.
[33] T. Mazanec, S. Perry, L. Tonkovich, Y. Wang, Nat. Gas Convers. Vii 147 (2004) 169.
[34] Y. Sun, Z. Jia, G. Yang, L. Zhang, Z. Sun, Int. J. Hydrogen energy 42 (2017) 29222.
[35] Y. Sun, G. Yang, L. Zhang, Z. Sun, Chem. Eng. Process Process Intensif. 119 (2017) 44.
[36] S. Mehta, V. Deshmane, S. Zhao, D. Kuila, Ind. Eng. Chem. Res. 53 (2014) 16245.
[37] R.Y. Abrokwah, M.M. Rahman, V.G. Deshmane, D. Kuila, Mol. Catal. 478 (2019) 110566.
[38] N. Mohammad, S. Bepari, S. Aravamudhan, D. Kuila, Catalysts 9 (2019) 872.
[39] A. Gavriilidis, P. Angeli, E. Cao, K.K. Yeong, S.S.Y. Wan, Chem. Eng. Res. Des. 80 (2002) 3.
[40] X. Ouyang, R. Besser, Catal. Today 84 (2003) 33.
[41] V. Hessel, P. Lob, H. Lowe, Stud. Surf. Sci. Catal. 159 (2006) 35.
[42] R. Guettel, T. Turek, Chem. Eng. Sci. 64 (2009) 955.
[43] A. Holmen, H.J. Venvik, R. Myrstad, J. Zhu, D. Chen, Catal. Today 216 (2013) 150.
[44] L. Han, D. Mao, J. Yu, Q. Guo, G. Lu, Catal. Commun. 23 (2012) 20.
[45] X. Sun, X. Zhang, Y. Zhang, N. Tsubaki, Appl. Catal. A Gen. 377 (2010) 134.
[46] Y. Zhang, S. Nagamori, S. Hinchiranan, T. Vitidsant, N. Tsubaki, Energy Fuels 20 (2006) 417.
[47] S. Bepari, R. Stevens-Boyd, N. Mohammad, Xin Li, R. Abrokwah, D. Kuila, Mater. Today (2020), https://doi.org/10.1016/j.matpr.2020.04.582.
[48] S.A. Salihi, R. Abrokwah, W. Dade, V. Deshmane, T. Hossain, D. Kuila, Int. J. Hydrogen Energy 45 (2020) 14183.
[49] R.Y. Abrokwah, W. Dade, S.L. Owen, V. Deshmane, M. Rahman, D. Kuila, Effects of Mesoporous Supports and Metals on Steam Reforming of Alcohols, E-Publishing, CRC, New York, 2019, pp. 93–106.
[50] A. Corma, M. Navarro, T. Perez-Pariente, J. Chem. Soc. Chem. Commun. (1994) 147.
[51] K.S.W. Sing, Pure Appl. Chem. 54 (1982) 2201.
[52] H.M. Gobara, Egypt. J. Pet. 21 (2012) 1.
[53] B. Huang, C.H. Bartholomew, S.J. Smith, B.F. Woodfield, Microporous Mesoporous Mater. 165 (2013) 70.
[54] V. Vosoughi, S. Badoga, A.K. Dalai, N. Abatzoglou, Fuel Process. Technol. 162 (2017) 55.
[55] G. Jacobs, Y. Ji, B.H. Davis, D. Cronauer, A.J. Kropf, C.L. Marshall, Appl. Catal. A Gen. 333 (2007) 177.
[56] G. Jacobs, T.K. Das, Y.Q. Zhang, J.L. Li, G. Racoillet, B.H. Davis, Appl. Catal. A Gen. 233 (2002) 263.
[57] J. Panpranot, J.G. Goodwin Jr., A. Sayari, Catal. Today 77 (2002) 269.
[58] S.K. Beaumont, S. Alayoglu, C. Specht, W.D. Michalak, V.V. Pushkarev, J. Guo, N. Kruse, G.A. Somorjai, J. Am. Chem. Soc. 136 (2014) 9898.
[59] W.C. Conner Jr., J.L. Falconer, Chem. Rev. 95 (1995) 759.
[60] J. Hong, E. Marceau, A.Y. Khodakov, L. Gaberova, A. Griboval-Constant, J.S. Girardon, C.L. Fontaine, V. Briois, ACS Catal. 5 (2015) 1273.
[61] S. Mandal, S. Maity, P.K. Gupta, A. Mahato, P. Bhanja, G. Sahu, Appl. Catal. A Gen. 557 (2018) 55.
[62] C.-H. Chen, C.-C. Huang, Microporous Mesoporous Mater. 109 (2008) 549.
[63] F. Roessner, U. Roland, J. Mol. Catal. A Chem. I12 (1996) 401.
[64] R. Kramer, M. Andre, J. Catal. 58 (1979) 287.
[65] T.N. Phaahlamohlaka, M.W. Dlamini, M.W. Mogodi, D.O. Kumi, L.L. Jewell, D.G. Billing, N.J. Coville, Appl. Catal. A Gen. 552 (2018) 129.
[66] G. Jacobs, W. Ma, B.H. Davis, Catalysts 4 (2014) 49.
[67] Y.P. Li, T.J. Wang, C.Z. Wua, X.X. Qin, N. Tsubaki, Catal. Commun. 10 (2009) 1868.
[68] D. Zhao, J. Feng, Q. Huo, N. Melosh, G. Fredrikson, B. Chmelka, G.D. Stucky, Science 279 (1998) 548.
[69] X.Y. Zhao, H.Y. Zhang, J. Chen, L.J. Li, Y.K. Liew, B.R.M. Nordin, Chem. Cat. Chem. 4 (2012) 265.
[70] V.R.R. Pendyala, G. Jacobs, W. Ma, J.L.S. Klettlinger, C.H. Yen, B.H. Davis, Chem. Eng. J. 249 (2014) 279.
[71] A. Sari, Chem. Eng. J. 244 (2014) 317.
[72] A. Haghtalab, A. Mosayebi, Int. J. Hydrogen Energy 39 (2014) 18882.
[73] K. Jalama, Catal. Commun. 74 (2016) 71.
[74] A. Monshi, M.R. Foroughi, M.R. Monshi, WJNSE 2 (2012) 154.
[75] C.H. Kwon, J.H. Kim, I.S. Jung, H. Shin, K.H. Yoon, Ceram. Int. 29 (2003) 851.
[76] N. Osakoo, R. Henkel, S. Loiha, F. Roessner, J. Wittayakun, Catal. Commun. 56 (2014) 168.
[77] J. Taghavimoghaddam, G.P. Knowles, J. A.L.Chaffee, Mol. Catal. A Chem. 358 (2012) 79.
[78] R.Y. Abrokwah, V.G. Deshmane, S.L. Owen, D. Kuila, Adv. Mat. Res. 1096 (2015) 161.
[79] V.G. Deshmane, R.Y. Abrokwah, D. Kuila, J. Mol. Catal. A. Chem. 408 (2015) 202.
[80] D.G. Castner, P.R. Watson, I.Y. Chan, J. Phys. Chem. 93 (1989) 3188.
[81] S.C. Petitto, M.A. Langell, J. Vac, Sci. Technol. A 22 (2004) 1690.
[82] A. Dinse, M. Aigner, M. Ulbrich, G.R. Johnson, A.T. Bell, J. Catal. 288 (2012) 104.
[83] H. Schulz, Catal. Today 214 (2013) 140.
[84] T.I. Sibianu, D. Berger, C. Matei, I. Calinescu, U.P.B. Sci. Bull. 78 (2016) 39.
[85] H. Schulz, E.V. Steen, M. Claeys, Stud. Surf. Sci. Catal. 81 (1994) 455.
[86] N. Mohammad, R.Y. Abrokwah, R.G. Stevens-Boyd, S. Aravamudhan, D. Kuila, Catal. Today (2020), https://doi.org/10.1016/j.cattod.2020.02.020.
[87] S. Zhao, V.S. Nagineni, N.V. Seetala, D. Kuila, Ind. Eng. Chem. Res 47 (2008) 1684.
[88] H. Schulz, Top. Catal. 26 (2003) 73.
[89] D.B. Bukur, X. Lang, A. Akgerman, Z. Feng, Ind. Eng. Chem. Res. 36 (1997) 2580.
[90] J. Chen, C. Yang, ACS Omega 4 (2019) 22237.